IV.3. PREPARATION OF δ-FeOOH. OXIDATION OF Fe^{2+} IN STRONGLY BASIC CONDITIONS. (Rongguang Lin, Robert L. Spicer and Burtron H. Davis)

IV.3.1. ABSTRACT

At a pH of about 14, it is possible to prepare essentially pure δ-FeOOH with a surface area of 100 m^2/g or greater even from Fe^{2+} solutions in the concentration range of 0.1 to 1M. A high rate of addition of oxidant and a low temperature favor the formation of δ-FeOOH; conversely, slow oxidation and high temperature favor the formation of α-FeOOH. It appears that the α-FeOOH is formed in competition with δ-FeOOH, and does not result from a secondary reaction of an initially formed δ-FeOOH. The rate of oxidation under the high pH conditions is limited by diffusion of the oxidant.

IV.3.2. INTRODUCTION

δ-FeOOH can be prepared from a ferrous salt (eg., $FeSO_4$) by rapid oxidation with, for example, an excess of 30% H_2O_2 at 60°C in a strongly basic medium (IV.3.1). According to this procedure, the initial concentration of Fe^{2+} should be low (< 0.01M) if one is to obtain pure δ-FeOOH. With a high initial concentrations of Fe^{2+} (> 0.1M), however, the oxidation product usually contains appreciable amounts of α-FeOOH (IV.3.2). Olewe *et al.* (IV.3.2) concluded that the formation of α-FeOOH takes place in at least two steps: the formation of its nucleus from δ-FeOOH and then the eventual growth of this nucleus. At a low concentration of Fe^{2+}, some of these nuclei do not advance due to the small size of the initial hydroxide particles, and hence this leads to the formation of δ-FeOOH. To prepare a large quantity of pure δ-FeOOH, this oxidation method needs to be modified so that high Fe^{2+} concentration may be employed.

Air oxidation of ferrous hydroxide in neutral or slightly basic solution can produce Fe_2O_3, Fe_3O_4, α-FeOOH, γ-FeOOH, or a mixture of these depending on, among others, the reaction temperature, oxidation rate, initial reactant concentration, pH and the initial molar ratio, $[Fe^{2+}]/[OH^-]$. Olewe (IV.3.2) studied the influence of concentration on the oxidation of ferrous hydroxide in basic sulphate medium and found that the amount of δ-FeOOH in the final product decreased with increasing initial concentration of $FeSO_4$. Little work has been done on the effect of reaction conditions on the final product of the oxidation of $Fe(OH)_2$ in a strongly basic solution. In addition, in order to obtain a specific end product, it is essential to have a clear understanding of the process of oxidation of $Fe(OH)_2$. An enormous amount of work has been done on the oxidation of Fe^{2+} in acidic and neutral solutions since the beginning of this century. The rate equations reported by various investigators for the oxidation of Fe^{2+} with oxygen and H_2O_2 are shown in Table IV.3.1 and IV.3.2, respectively. It has been shown that the rate of iron oxidation depends on the concentration of ferrous ion, the oxidizing agent, and the pH of the solution (IV.3.4-IV.3.12).

In an acidic solution (pH below 3), oxidation proceeds very slowly, and the rate is independent of pH. [It should be noted that, in most cases referred to in this introduction, not all of the iron is in solution]. McBain (IV.3.13) found that the oxidation under these conditions is first order with respect to oxygen and second order with respect to ferrous ion concentration ([ ] represents molar concentration):

$$-\frac{d(Fe^{2+})}{dt} = k[Fe^{2+}]^2[O_2] \qquad \text{[IV.3.1.]}$$

In a slightly acidic solution (pH 3-5), oxidation proceeds more rapidly than in the more acidic solution. Holluta and Kölle (IV.3.14) observed that oxidation is first order with respect to ferrous ion and oxygen, and also in hydroxide ion:

$$-\frac{d[Fe^{2+}]}{dt} = k[Fe^{2+}][O_2][OH^-] \qquad \text{[IV.3.2.]}$$

In a nearly neutral solution (pH range of 6-8), the reaction rate is much higher. Just (IV.3.12) and Stumm (IV.3.15) reported the rate equation as:

$$-\frac{d[Fe^{2+}]}{dt} = k[Fe^{2+}][O_2][OH^-]^2 \qquad \text{[IV.3.3.]}$$

Tamura *et al.* (IV.3.10) found that the oxidation of Fe^{2+} in a neutral solution is accelerated by the reaction product; this applies to all forms of Fe^{3+} hydroxide, including α-FeOOH, ß-FeOOH and γ-FeOOH. At constant pH and O_2 concentration, the rate of oxidation can be expressed as:

$$-\frac{d[Fe^{2+}]}{dt} = (K + K')[Fe^{3+}][Fe^{2+}] \qquad \text{[IV.3.4.]}$$

where K is the rate constant for the homogeneous reaction that occurs in solution and K' is the rate constant for the heterogeneous reaction that is catalyzed by Fe^{3+} hydroxide. Prasad and Ramasastry (IV.3.16) studied the air-oxidation of a $Fe(OH)_2$ suspension at room temperature. They found that a straight line was obtained by plotting $\log([Fe^{3+}]/[Fe^{2+}])$ against time. They reported a rate equation for the aerial oxidation of a $Fe(OH)_2$ suspension as:

$$-\frac{dx}{dt} = \frac{kx(a-x)}{a} \qquad \text{[IV.3.5.]}$$

where a is the initial amount of ferrous hydroxide present in a given volume of the suspension; x is the amount of ferric hydroxide formed at a time, t; a-x is the amount of Fe^{2+} at time t. This means that the rate of reaction is a function of the amount of Fe^{2+} and Fe^{3+} present in the suspension. However, they did not provide an explanation for these observations.

Similarly, the oxidation of Fe^{2+} by H_2O_2 in an acidic solution has been extensively studied (IV.3.17-IV.3.28). The rate of oxidation is first order with respect to the concentration of Fe^{2+} and OH^-. In acidic solution, the mechanism of the oxidation reaction has been represented to occur by the following steps:

$$Fe^{2+} + H_2O_2 \rightarrow Fe^{3+} + OH\cdot + OH^- \qquad \text{[IV.3.6.]}$$

$$Fe^{2+} + OH\cdot \rightarrow Fe^{3+} + OH^- \qquad \text{[IV.3.7.]}$$

$$OH\cdot + H_2O_2 \rightarrow HO_2\cdot + H_2O \qquad \text{[IV.3.8.]}$$

$$Fe^{2+} + HO_2\cdot \rightarrow Fe^{3+} + HO_2^- \qquad \text{[IV.3.9.]}$$

$$Fe^{3+} + HO_2\cdot \rightarrow Fe^{2+} + O_2 + H^+ \qquad \text{[IV.3.10.]}$$

When the ratio $[H_2O_2]/[Fe^{2+}]$ is low, reactions 6 and 7 dominate, a second order rate law is operative, and O_2 is not evolved. As the ratio of $[H_2O_2]/[Fe^{2+}]$ increases, steps 9 and 10, competing for the $HO_2\bullet$ radical, become the dominant reaction. Thus, oxidation of Fe^{2+} dominates initially but the decomposition of H_2O_2 becomes more important as the concentration of H_2O_2 increases. Recently, Millero et. (IV.3.25)

studied the dependence of the reaction on pH and found that the rate of oxidation increases with increasing pH. This increase in rate was considered to be connected with the formation of $Fe(OH)_2$ (aq), which is more reactive than the Fe^{2+} ion.

In a strongly basic solution, however, the kinetics of oxidation of the iron(II) hydroxide by H_2O_2 has not been reported. This may reflect the difficult of making kinetic studies in a strongly basic solution because of complications caused by the decomposition of H_2O_2 in the presence of ferric hydroxide. In the present study, the preparation of δ-FeOOH by adding H_2O_2 at various flow rates and with high ($\sim$0.6M) Fe^{2+} concentrations has been studied. The advantage of this approach is that the oxidation rate can be controlled by the flow of H_2O_2 so that this method can be used to study the effect of the rate of addition of the oxidant on the phase composition of the final product. This study was designed to: (1) define the optimum condition for the preparation of pure δ-FeOOH by H_2O_2 oxidation and (2) investigate the possibility of replacing H_2O_2 with O_2 or air to prepare δ-FeOOH. The behavior of Fe^{2+} hydroxide oxidation in strongly basic solution by H_2O_2 and oxygen was compared. If the procedure is to have utility as a method for catalyst preparation, it is necessary to operate at reasonably high iron concentrations. Thus, high Fe^{2+} concentrations have been employed.

IV.3.3. EXPERIMENTAL

IV.3.3.a. Materials

Melanterite ($FeSO_4 \cdot 7H_2O$), KOH and 30% H_2O_2 were ACS reagent grade and were purchased from Aldrich. The iron salt was stored in a desiccator to prevent oxidation. A 0.1 N $KMnO_4$ solution was also purchased from Aldrich and standardized

using known concentration of $H_2C_2O_4$ solution. To obtain data for mass balance calculations, the concentration of H_2O_2 was determined by titration with a 0.1 N $KMnO_4$ solution.

IV.3.3.b. Apparatus

The experiments were conducted in a 2000 mL five-neck spherical flask into which a pH electrode, stirrer, thermometer, glass gas dispersion tube for oxygen or teflon tube for H_2O_2 were inserted; the remaining neck was used to make a connection to a rotameter or a flowmeter. The reaction vessel was placed in a water or ice bath so that the reaction could be carried out at a fixed, constant temperature.

IV.3.3.c. Methods

After adding 1000 mL of deionized water to the 2 L reaction flask, which was placed in an ice bath, argon gas was bubbled through the water (stirred at 600 r.p.m.) for 30 min. to remove any dissolved carbon dioxide and oxygen, and then 166.81 g of $FeSO_4 \cdot 7H_2O$ was added and stirred under argon flow until the $FeSO_4$ was dissolved completely. Then solid KOH was added to the flask to give a molar ratio of $[Fe^{2+}]/[OH^-]$ of 0.4. The suspension was stirred for 15 minutes under argon until the pH of the suspension became constant. The temperature was controlled at 0°C unless noted otherwise. Hydrogen peroxide (30%) was then pumped at a fixed rate into the suspension using a syringe pump. For the experiments with oxygen, a controlled flow of the gas was bubbled into the suspension through a gas dispersion tube (75-100 μm). Reaction time was measured from the start of introduction of oxygen or hydrogen peroxide solution. During oxidation, the pH remained constant at 14. All experiments were conducted at atmospheric pressure.

The studies of the oxidation rate of ferrous hydroxide were performed by monitoring the change in the molar fraction, Fe^{2+}/Fe_{total}, and the oxygen evolution rate with time during the reaction. Therefore, during the course of the oxidation, samples were removed by a syringe at appropriate intervals and added to a hot acid solution (20 mL of concentrated HCl and 50 mL of 1M sulfuric acid) to quench the oxidation reaction since the ferrous ion is very stable with respect to oxidation in a strong acidic solution. The excess HCl, which may interfere in the subsequent titration with $KMnO_4$, was removed by evaporating the solution to a volume less than 30 mL. The solution was then transferred to a volumetric flask and diluted to 200 mL with deionized water. Fe^{2+} was determined by titrating an aliquot of the iron solution with standard $KMnO_4$ solution and total iron was analyzed by titration with standard $KMnO_4$ solution after reduction of Fe^{3+} to Fe^{2+} using amalgamated zinc in a Jones Reductor (IV.3.10).

After the reaction was complete, the oxidation product was collected by filtration. The solid was washed with deionized water several times until SO_4^{2-} was not detected in the filtrate when $BaCl_2$ was added. The filter cake was then washed with acetone to remove most of the water. The precipitate was dried under vacuum at room temperature for 24 hrs.

The X-ray diffraction pattern of the product was measured using Cu K_α (1.5418 Å) radiation (40 KV and 20 mA) with a Philips X-ray diffractometer. The data were collected using a VMS/VAX 700 system. The identification of products was accomplished by matching the diffraction peak positions and intensities with standards contained in the ASTM data files.

IV.3.4. RESULTS

IV.3.4.a. Oxidation with H_2O_2

When hydrogen peroxide was added to the suspension at a fixed rate, the $Fe(OH)_2$ was oxidized and the color of the suspension changed from white to green and finally to a dark brown. The molar fraction of Fe^{2+} in the samples withdrawn at increasing times are collected in Table IV.3.3. Plots of Fe^{2+}, as percentage of the initial Fe^{2+} concentration, versus time (Figure IV.3.1) show that Fe^{2+}% decreases linearly with time. The slopes (oxidation rates) obtained from the lines in Figure IV.3.1 are proportional to the H_2O_2 flow rate (FR (mL/min.)); the relation between FR and oxidation rate is:

$$Oxidation\ rate = \frac{1}{t} = 0.034FR \qquad \textbf{[IV.3.11]}$$

where t is the reaction time.

The oxidation of Fe^{2+} (mmol/min) increases linearly with flow rate (Figure IV.3.2), and the slopes show that the oxidation of $Fe(OH)_2$ by H_2O_2 proceeds according to the stoichiometric relation:

$$2Fe(OH)_2 + H_2O_2 \rightarrow 2FeOOH + 2H_2O \qquad \textbf{[IV.3.12.]}$$

Gaseous oxygen, resulting from decomposition of H_2O_2, was not observed until the reaction was essentially complete (Figure IV.3.3). Thus, H_2O_2 reacts with $Fe(OH)_2$ at a much faster rate than it decomposes to oxygen. This is true even though the rate of oxygen formation after all of the Fe^{2+} has been oxidized is only about 30 times slower than the oxidation of Fe^{2+} prior to the formation of gaseous oxygen.

IV.3.4.b. Oxidation with oxygen

The nature of the reaction of Fe^{2+} with oxygen is similar to that with hydrogen peroxide. However, the percentage of Fe^{2+} converted is not linear with time (Figure IV.3.4). At the beginning of the oxidation, the decrease in Fe^{2+} is slow (apparent induction period), then increases with time, and toward the end of the reaction, the oxidation rate slows again. The exit oxygen flow rate changes during the oxidation (Figure IV.3.5). Initially the flow decreases to a minimum value and remains nearly constant until the reaction of Fe^{2+} is nearly complete. The time required for the oxygen flow to reach a minimum value is approximately equal to 5 to 10 times the volume of the fraction of the flask that is not filled with solution (V_R, the difference between the volume of the flask and the volume of the suspension). When the reaction is nearly complete, the exit gas flow increases until the inlet and the outlet flow of oxygen are equal (Figure IV.3.5). The "induction" period is reduced by increasing the oxygen flow (Figure IV.3.5). However, this induction period, which has been reported by others, is, in our study, due to reactor design. Decreasing V_R results in either the elimination, or at least a great reduction, of the induction period. The induction period is therefore due to the time needed to sweep the inert gas blanket from the dead space of the gas inlet line and reactor void, V_R. As with oxidation with H_2O_2, an increase in the oxygen flow leads to a decrease in the time for complete Fe^{2+} conversion.

The data for the amount of ferrous hydroxide (mmole) oxidized during a given time interval for three oxygen flow rates (75, 185 and 390 mL/min.) are collected in Table IV.3.4. The oxidation rate of ferrous hydroxide (mMole/min) with increasing

reaction time for an oxygen flow rate of 185 mL/min shows that the oxidation rate during the induction period is low, and after this period the oxidation rate remains constant until near the end of the reaction.

IV.3.4.c. Effect of Flow Rate and Temperature on the Product

The products obtained by the oxidation of the ferrous hydroxide suspension with H_2O_2 or oxygen are δ-FeOOH or a mixture of α-FeOOH and δ-FeOOH, depending upon the flow rate of the oxidant and the reaction temperature. At 0°C, an increase in flow rate results in an increase in the fraction of δ-FeOOH in the product (Figures IV.3.6 and IV.3.7). On the other hand, an increase in the reaction temperature leads to a decrease in the fraction of δ-FeOOH. The X-ray diffraction patterns (Figure IV.3.8) show that the phase composition of the product changes when all reaction conditions are maintained the same except temperature (0°C or 16°C). After δ-FeOOH is formed, it is stable since the transformation of δ-FeOOH to α-FeOOH did not occur when a suspension of δ-FeOOH was heated at 70°C for up to 90 min. (Figure IV.3.9).

XRD patterns of δ-FeOOH contain four main peaks whose width follows the order $100 \simeq 110 < 101 < 102$ indicating a preferred crystal growth in a direction corresponding to the c direction of the δ-FeOOH crystal. The surface area of the products following drying at room temperature ranged from about 110 to 200 m^2/g.

A series of samples were prepared at 0°C using a range of flow rates of H_2O_2 or O_2. These preparations were carried out in a continuous stirred tank reactor (CSTR) with a constant amount of iron and a continuous flow of the oxidant. The Fe^{2+}/OH^- ratio was 0.4 and a 1.0M Fe^{2+} slurry was used. Thus, the conversion, based

on iron, was conducted in a batch reactor in which the Fe^{2+} concentration decreased continuously with a concurrent increase in the Fe^{3+} concentration. The oxidant, O_2 or H_2O_2, was added continuously so that an unknown, but steady-state concentration of the oxidant should be established.

For oxidation with H_2O_2 the surface area of the final product appears to increase as the flow rate increases, and attains an ultimate value of about 150-160 m^2/g (Table IV.3.5). With oxygen, the surface area appears to be maximum at the lower flows, and to attain a level of about 200 m^2/g. Additional study would be required to verify that the apparent decrease in surface area at the highest flow of oxygen is valid. The flow of H_2O_2 and O_2 were chosen so that the total number of electron acceptors added during the same time interval would be equivalent. In both cases, the oxidant was consumed in converting Fe^{2+} since H_2O_2 did not decompose to produce oxygen and all of the oxygen added to the CSTR reacted until essentially all of the iron was converted.

In general, the Broekhoff-deBoer (IV.3.30,IV.3.31) porosity provided the best agreement between the BET surface area and the area calculated using the pore model. Consequently, this model has been utilized for calculating the pore size distribution. The pore size of maximum volume is largest for the lowest H_2O_2 flow. The pore size of maximum volume decreases as the rate of addition of H_2O_2 is increased and then may become larger as the flow continues (Figure IV.3.10). In general, the adsorption isotherm and hysteresis loop do not show a dramatic dependence upon the rate of H_2O_2 addition (Figure IV.3.11). Likewise, for a common

rate of oxidant addition, there does not appear to be significant difference in the material produced by oxidizing with H_2O_2 or with O_2.

A series of catalysts were prepared to determine the effect of aging at 70°C on the crystal phase, particle size, surface area and porosity of a δ-FeOOH prepared at 25-30°C. This was done to determine whether α-FeOOH forms directly at the higher temperatures or was a result of a transformation of the δ-FeOOH that forms initially. A viscous greenish-white slurry was produced from 125g $FeSO_4 \bullet 7H_2O$, dissolved in 200 mL deionized water, and 175 mL KOH (7.3M). The suspension was cooled 25°C and the pH was 12.5. During about 40 min. 280 mL cooled H_2O_2 (30%) was added in 40 mL increments spaced so as to maintain the temperature below 30°C. After all of the H_2O_2 had been added, a portion of the slurry was collected by filtration, washed twice with 300 mL deionized water, and the wet cake was dried in an oven at 70°C overnight. The other portion of the slurry was heated to 70°C during 5 minutes and maintained at this temperature. At time intervals, 40 mL aliquots were withdrawn and added to 100 mL cooled deionized water. The solid was collected by filtration, washed with deionized water and then acetone, and dried in air. The filtration was much faster if the washing utilized 2M NH_4NO_3 rather than deionized water. The only phase detected by X-ray diffraction in the unaged and aged samples was δ-FeOOH. There was a drop in surface area from 137 to 113 m^2/g during the first 10 minutes of heating and then essentially no charge occurred with an additional 80 minutes of heating (Figure IV.3.12). However, during the heating period at least some of the crystallite sizes obtained from X-ray line broadening undergo change (Figure IV.3.12). Thus, there is a continuous decrease in the crystal size in the directions

corresponding to the 100, 101 and 102 planes; however, the size corresponding to the 112 plane does not undergo a change during the heating period. Thus, the size corresponding to the 100 plane decreases from about 19.6 to 15.7 nm while the size corresponding to the 112 plane remains constant at 14.9 nm. The crystal size corresponding to the 102 plane is much smaller but still declines from 5.4 nm to 4.3 nm during 90 minutes. Thus, there is a decided crystal preference for the changes that occur with aging at 70°C.

The surface area of samples of δ-FeOOH that were calcined in air for 16 hours remains the same with heating to 150°C, there is an increase in surface area to attain a maximum at about 200°C and then a gradual decline in area with higher calcination temperatures (Figure IV.3.13).

IV.3.5. DISCUSSION

IV.3.5.a. Preparation

Our results show that oxidation of $Fe(OH)_2$ in a strongly basic suspension can produce α- and/or δ-FeOOH, and that nearly pure δ-FeOOH can be formed for Fe^{2+} concentrations at high as 1M. The formation of δ-FeOOH from $Fe(OH)_2$ by rapid oxidation with hydrogen peroxide has been considered to be a topotactic transformation between two solid phases of hexagonal close-packed structure (IV.3.32-IV.3.34). Since δ-FeOOH has the same structure as the $Fe(OH)_2$ crystal, it is conceivable that rapid oxidation favors the formation of δ-FeOOH. This mechanism requires the oxidation to occur in the solid phase, and not in the solution. On the other hand, it has been proposed that the mechanism for the formation of α-FeOOH from air oxidation of $Fe(OH)_2$ in a basic solution is a dissolution/reprecipitation

process, and slow oxidation therefore favors the formation of the more stable α-FeOOH (IV.3.32).

Our preliminary experiments in the preparation of δ-FeOOH revealed that the phase that is formed is very sensitive to small variations in the method used for the synthesis. The temperature and flow rate of hydrogen peroxide have an effect on the phase composition of the product. At constant temperature, an increase in flow rate of H_2O_2 favors the formation of δ-FeOOH while at a constant flow rate, a decrease in reaction temperature favors the formation of δ-FeOOH. In other words, low temperature and high flow rate of H_2O_2 are needed to produce pure δ-FeOOH. Our results suggest that, for an 0.6M Fe^{2+} suspension, a flow rate of 1.7 mL/min. H_2O_2 (30%) is sufficient to produce essentially pure δ-FeOOH at 0°C.

It has been reported that δ-FeOOH can be converted to α-FeOOH in a basic solution at high temperature (>120°C) (IV.3.33). However, the α-FeOOH phase that we obtained at 16°C cannot be simply explained by a temperature effect since the δ-FeOOH that was formed at 0 to 30°C was stable upon heating the suspension at 70°C for at least 90 minutes. The formation of α-FeOOH in the present studies must therefore occur in competition with δ-FeOOH during the oxidation, and not from the transformation of the initial, δ-FeOOH.

Like hydrogen peroxide, an increase of flow rate of oxygen results in an increase in the fraction of δ-FeOOH in the solid. For the present conditions, the final product contains a small amount of α-FeOOH even with the highest oxygen-flow rate (780 mL/min, oxidatively equivalent to 6.7 mL/min. flow rate of H_2O_2 (10.2 M)) used in this study. Thus, for a 0.6M Fe^{2+} suspension at a pH about 14, an oxidation rate of

0.017M/min. is sufficient to produce essentially pure δ-FeOOH. This has been explained as follows. When the Fe^{2+} hydroxide particles are contacted by oxygen, the outer layers of the particles form δ-FeOOH. The dense layers of δ-FeOOH prevent egress of oxygen to inner layers of Fe^{2+} hydroxide particles. Since the thickness of δ-FeOOH layer increases with reaction time, the oxygen supply may be insufficient to oxidize the inner layers of Fe^{2+} hydroxide particles, resulting in a decrease in oxidation rate and, in turn, the formation of α-FeOOH. In the case of hydrogen peroxide, δ-FeOOH formed is not necessarily concentrated near the surface of the $Fe(OH)_2$ particles. Hence, the δ-FeOOH formed from $Fe(OH)_2$ by rapid oxidation with H_2O_2 readily cracks, giving rise to a path for H_2O_2. In other words, the δ-FeOOH layer cannot be protective for further oxidation of inner layer of $Fe(OH)_2$ (IV.3.7). In the present case it appears that the constant reaction rate and the inability to attain a rate of H_2O_2 addition great enough to reach a limiting reaction rate suggest that the reaction occurs in the solution rather than the solid.

IV.3.5.b. Kinetic behavior

IV3.5.b.1. Oxidation with hydrogen peroxide

The fact that the percentage of Fe^{2+} decreases linearly with time of peroxide flow indicates that oxidation occurs in the liquid phase and not on the surface of the solid phase. If the solid phase reaction is predominant, the decrease in Fe^{2+} percentage should be represented by a parabolic law since the oxidation rate would decrease with an increase in the thickness of the FeOOH layer on the particles of $Fe(OH)_2$ (IV.3.8). Hence, it is concluded that the oxidation of the suspension takes place in the liquid phase. Furthermore, the suspension is saturated with respect to

Fe^{2+}. When H_2O_2 is pumped into the suspension, the Fe^{2+} ions in solution react with H_2O_2, giving rise to the formation of δ-FeOOH. When the suspension is well mixed, the ferrous ions consumed by oxidation are replaced by dissolution of the precipitate of $Fe(OH)_2$ so that the concentration of ferrous ion in the suspension remains constant during essentially all of the oxidation process.

The slopes in Figure IV.3.1 depend on the flow rate of hydrogen peroxide, which means that the oxidation rate depends on the flow rate of hydrogen peroxide. To determine the reaction order with respect to H_2O_2, we assume that the concentration of hydrogen peroxide in the suspension is proportional to the flow rate of hydrogen peroxide. Hence, at constant pH and concentration of Fe^{2+}, the rate law of the oxidation with H_2O_2 is represented by:

$$dx/dt = -k[FR]^n \qquad \textbf{[IV.3.13.]}$$

where x is the molar fraction of Fe^{2+}; FR is the flow rate of H_2O_2; n is the reaction order for H_2O_2; and k is the rate constant. Integrating equation IV.3.14, we obtain:

$$x_o - x_t = k[FR]^n t \qquad \textbf{[IV.3.14.]}$$

where $x_0 = 1$ and x_t is the molar fraction of ferrous hydroxide at time t. When $x_t = 0.5$, $t = t_{1/2}$, and equation IV.3.15 can be written

$$0.5/t_{1/2} = k[FR]^n \qquad \textbf{[IV.3.15.]}$$

or

$$1/t_{1/2} = 2k[FR]^n \qquad \text{[IV.3.16.]}$$

A plot of $\ln[1/t_{1/2}]$ versus ln[FR] should be a straight line with a slope n and intercept of ln(2k), and it is (Figure IV.3.14). From the intercept and slope of this line, we obtain n = 1 and ln(2k) = -2.6, which means that oxidation of $Fe(OH)_2$ with H_2O_2 is first-order with respect to H_2O_2 with a rate constant k of 0.037(mL^{-1}). Likewise, the constant slope in Figure IV.3.1 for each H_2O_2 flow rate indicates that the reaction is zero order for Fe^{2+}.

IV3.5.b.2. Oxidation with oxygen

The experimental results show that oxidation is slow during the early stage. Tiwar (IV.3.35) considered this to represent an induction period. However, it appears that the "induction period" in the present study is due to the experimental design. To prevent oxidation of the Fe^{2+} prior to the start of the oxygen flow, the system is blanketed with argon. There is a volume of argon (V_R) in the dead space of the reaction flask above the $Fe(OH)_2$ suspension and in the gas delivery lines. Under conditions of no reaction it would require a flow of oxygen of about 5 V_R before the gas in the dead space of the flask would be > 99% O_2; since oxygen reacts with Fe^{2+} it will take an oxygen flow of greater than 5 V_R before the gas in the reaction vessel is pure oxygen. It therefore appears that the decline in oxygen flow from the reactor, and the corresponding increase in oxidation rate of Fe^{2+}, is due to the time required to replace the argon in the dead space with oxygen so as to produce a steady state condition. The fact that the induction period decreases with increasing oxygen flow rate as well as the decrease in induction period as the dead volume (V_R) is decreased support this explanation.

The linear rate of oxidation of Fe^{2+} by oxygen following the "apparent induction period" indicates that oxidation is independent of the relative amounts of Fe^{2+} or Fe^{3+} present in the suspension as the oxidation proceeds.

The amount of oxygen that reacted with Fe^{2+} is equal to the difference between the amount of oxygen added and the amount of unreacted oxygen; this is, the flow of oxygen that reacted (FR') can be represented as:

$$FR' = FR - FR'' \qquad \textbf{[IV.3.17.]}$$

where FR is the flow rate of oxygen added to the suspension (mL/min) and FR" is the flow rate of oxygen exiting the suspension (mL/min). It is assumed that FR' is proportional to the concentration of oxygen in the suspension.

Similar to hydrogen peroxide, plotting $\ln(1/t_{1/2})$ versus ln(FR') should produce a straight line with a slope of n and an intercept of ln(2k). The slope of the line in the ln-ln plot is 1 and the relation between $(1/t_{1/2})$ and FR' is:

$$\ln(1/t_{1/2}) = \ln(FR') - 7.7 \qquad \textbf{[IV.3.18.]}$$

Hence, the oxidation rate is first order with respect to oxygen and the observed rate constant obtained from the intercept in Figure IV.3.12 is 2.3×10^{-4} mL^{-1}.

A reaction order of one cannot be assigned with certainty unless diffusional effects can be eliminated. In the present study, the hydrogen peroxide did not undergo decomposition to produce oxygen even though this was easily observed during the period following the oxidation of Fe^{2+}. For the quenched samples, withdrawn at various reaction times, unreacted H_2O_2 was not detected. Even at the most rapid flow rate of H_2O_2, the reaction rate remained constant as the Fe^{2+} was converted and there was no evidence for a rate increase with reaction time due to an

increase in H_2O_2 concentration at later reaction times. The above observations suggest that the first order rate in H_2O_2 means the rate limiting step is due to diffusion of the oxidant. The oxidation with gaseous oxygen also appears to be diffusion limited.

The steady-state rate may be written either in terms of the transport across the gas-liquid boundary or in terms of the reaction in solution. These expressions are, respectively:

$$r_d = k_m a_m (C_{1,g} - C_{1,L}) \qquad \textbf{[IV.3.19.]}$$

$$r_r = k_r C_{1,L}^n C_{2,L}^m \qquad \textbf{[IV.3.20.]}$$

where $C_{1,g}$ and $C_{1,L}$ are the oxygen concentrations in the gas and liquid, respectively; k_m is the mass-transfer coefficient between bulk and liquid; a_m is the gas-liquid interface area; k_r is the reaction rate, $C_{2,L}$ is the concentrations of Fe^{2+} in the solution and m and n are the reaction order with respect to Fe^{2+} and oxygen, respectively. Consider the case where the rate of reaction is very much greater than $k_m a_m$. Under this condition $C_{1,L}$ approaches zero and equation IV.3.21 becomes:

$$r_d = k_m a_m C_{1,g} \qquad \textbf{[IV.3.21.]}$$

This situation would explain the observed data where the rate was first order with respect to the oxidant and zero order with respect to Fe^{2+} and Fe^{3+}. The experimental rates obtained at the high pH are therefore at variance with the rate equations compiled in Tables IV.3.1 and IV.3.2.

Data (IV.3.36-IV.3.40) for half-life measurements for the oxidation of Fe^{2+} in the pH range from about 4 to 8 are plotted in Figure IV.3.15. Extrapolation of this data to

a pH of 14 suggest a half of 10^{-14} sec. for our reaction conditions. A reaction that is this rapid would certainly be diffusion limited under our experimental conditions.

It appears that the oxidation results are better explained by a mechanism involving dissolved Fe^{2+} species rather than oxidation of a solid, crystalline $Fe(OH)_2$. Thus, the crystal phase that is obtained depends upon the concentration of Fe^{3+} in the solution which influences the seed crystal structure that is formed as well as the rate of crystal growth. It appears that the more stable α-FeOOH is produced when the solution concentration of Fe^{3+} is low. Likewise, a higher temperature favors the formation of the more stable α-FeOOH form.

IV.3.6. SUMMARY

The rate of addition of the oxidant and the reaction temperature affect the final product of oxidation of $Fe(OH)_2$ by either H_2O_2 or O_2. A high rate of addition of oxidant and a low temperature are needed for the formation of δ-FeOOH; α-FeOOH is produced at low flow rate and/or high temperature. The rate of the oxidation with H_2O_2 depends on the flow rate of H_2O_2 and is independent of the ratio of ferrous and ferric hydroxide present in the suspension. With oxygen oxidant, the rate appears to depend on the transfer rate of oxygen from gas to liquid phase. While the reaction is first order in oxidant for the conditions of the present study, this order is apparently the result of diffusion limitations.

IV.3.7. ACKNOWLEDGMENT

The authors acknowledge the financial support of this work by the Department of Energy contract No. DE-AC22-91PC90056 and by the Commonwealth of Kentucky.

IV.3.8. REFERENCES

IV.3.1. Muller, O.; Wilson, R.; Krakow, W. *J. Materials Science* 1979, **14**, 2929.

IV.3.2. Olewe, A.A.; Refait, P.; Génin, J.M. *Corrosion. Sci.* 1991, **32**, 1003.

IV.3.3. Cheielewski, T. Charewicz. W.A. *Hydrometallurgy* 1984, **12**, 21.

IV.3.4. Huffmann, R.E.; Davison, N. *J. Am. Chem. Soc.* 1956, **53**, 4836.

IV.3.5. Cornelius, R.J.; Woodcock, J.T. *Proc. Aust. Inst. Min. Met.* 1958, **185**, 65.

IV.3.6. Keenan, E.A. Ph.D. Thesis, University of New South Walse, 1969.

IV.3.7. Mathews, C.T.; Robins, R.G. *Proc. Aust. Inst. Min. Met.* 1972, **242**, 47.

IV.3.8. McKay, D.R.; Halpern. *J. Trans. Metall. Soc. AIME* 1958, **212**, 301.

IV.3.9. Cher, M.; Davison, N. *J. Am. Chem. Soc.* 1955, **77**, 793.

IV.3.10. Tamura, H., Goto K., Nugayama, M. *Corrosion Sci.* 1976, **16**, 197.

IV.3.11. George, P. *J. Chem Soc.* 1954, **4**, 4349.

IV.3.12. Just, G. *Z. Physik. Chem.* 1908, **63**, 385.

IV.3.13. McBain, J.W. *J. Phys. Chem.* 1901, **5**, 623.

IV.3.14. Holluta, J.; Kölle, W. *Das Gas und Wasserfach.* 1964, **18**, 471.

IV.3.15. Stumm. W.; Lee, G.F. *Ind. Eng. Chem.* 1961, **53**, 143.

IV.3.16. Prasad, T.P.; Ramasastry, V.V. *J. Appl. Chem. Biotechnol.* 1977, **27**, 409.

IV.3.17. Haber, F.; Weiss, J. *Proc. R. Soc. London, Ser. A.* 1934, 332.

IV.3.18. Barb. W.G.; Baxendale, J.H.; Hargrove, K.R. *Trans. Faraday Soc.* 1951, **47**, 591.

IV.3.19. Hardwick, T.J. *Can. J. Chem.* 1957, **35**, 428.

IV.3.20. Wells, C.F.; Salam, M.A. *Trans. Faraday Soc.* 1967, 620.

IV.3.21. Wells, C.F.; Salam, M.A. *J. Chem. Soc. (A)* 1968; 24.

IV.3.22. Po, H.N.; Sutin, N. *Inorg. Chem.* 1968, **7**, 621.

IV.3.23. Skinner, J.F.; Glasel, A. Hsu, L.C.; Funt, B.L. *J. Electrochem. Soc.* 1980, **127**, 315.

IV.3.24. Moffett, J.W.; Zika, R.G. *Environ. Sci. Technol.* 1987, **21**, 804.

IV.3.25. Millero, F.J.; Sotolongo, S. *Geochim. Cosmochim. Acta* 1989, **53**, 1867.

IV.3.26. Baxendale, J.H.; Evans, M.G.; Park, G.S. *Trans. Faraday Soc.* 1947, **42**, 155.

IV.3.27. Rigg, T.; Taylor, W.; Weiss, J. *J. Chem. Phys.* 1954, **22**, 575.

IV.3.28. Dainton, F.S.; Sutton, H.C. *Trans. Faraday Soc.* 1953, **49**, 1011.

IV.3.29. Vogel, A. (ed.) (1978). "Textbook of Quantitative Inorganic Analysis," 4th edn. London and New York; Longman.

IV.3.30. Broekhoff, J. C. P.; deBoer, J. H. *J. Catal.* 1967, **9**, 8, 15.

IV.3.31. Broekhoff, J. C. P.; deBoer, J. H. *J. Catal.* 1968, **10**, 368, 377.

IV.3.32. Bernal, J.D.; Dasgupta, D.A.; Mackay, A.L. *Clay Miner. Bull.* 1959, **4**, 15.

IV.3.33. Feitknecht, W. *Z. Electrochem.* 1959, **67**, 1850.

IV.3.34. Okamotyo, S.J. *J. Soc. Chem. Ind. Japan* 1964, **67**, 1850.

IV.3.35. Tiwari, B.L.; Kolbe, J.; Hayden, Jr., H.W. *Metallurgical Transaction B* 1979, **10B**, 607.

IV.3.36. Singer, P. C.; Stumm, W. *Science*, 1970, **167**, 1121.

IV.3.37. Ghosh, M. M. "Aqueous-Environmental Chemistry of Metals," (Rubin, A. J., ed.) Science Pub., Ann Arbor, MI, 1974, pp 193-217.

IV.3.38. Davison, W.; Seed, G. *Geochim. Cosmochim. Acta* 1983, **47**, 67.

IV.3.39. Rockens, E. J.; van Grieken, R. E. *Marine Chem.* 1983, **13**, 195.

IV.3.40. Eary, L. E.; Schramke, J. A. "Chemical Modeling in Aqueous Systems. II," (D. C. Melchior and R. L. Bassett, eds.) ACS, Washington, DC, 1990, pp 379-396.

Table IV.3.1
The literature data on Fe^{2+} oxidation with oxygen in aqueous solution.

Reference	Kinetic equation $d[Fe^{3+}/dt = r =$	Rate Constant, k	Condition for the Study	Activation energy, kJ/M
Cheiclewski and Charewicz[3] (1984)	$r = k[Fe^{2+}]^2 p_{O2}$ exp(-519/RT)	0.0091-1.27 (l/mole min)	$[Fe^{2+}]$=>3.8 g/L Batch P_{O_2}: 132-1000 kPa $[Fe_T]$: Atomic Absorption $[Fe^{2+}]$: potentiometric titration T: 313-408K	57
Huffmann and Davidson[4] (1956)	$r = k[Fe^{2+}]^2 p_{O2}$	2.78×10^{-6} M^{-1} $atm^{-1}sec^{-1}$	1F H_2SO_4 Flow method Spectrophotometric method T: 304K	67.9
Cornelius and Woodcock[5] (1958)	$r=k[Fe^{2+}]^2[O_2]$		T: 373-403K	62.0
Keenan[6] (1969)	$r=k[Fe^{2+}]^2[O_2]^{1.04}[H^+]^{-0.35}$		T: 293-323 K	94.1
Mathews and Robins[7] (1972)	$r = k[Fe^{2+}]^2[O_2][H^+]^{-0.25}$ exp(-17.6X10^{-3}/RT)	1.32×10^{11}	$[Fe^{2+}]$:0.01-1 M pH: 0-2 Flow method Flow rate: 0.5 L/min Spectrophotometric method for Iron analysis T:293-353 K	73.7
McKay and Halpern[8] (1958)	$r = k[Fe^{2+}]^2 p_{O2}[Cu(II)]^{0.25}$		T: 373-403	69.1
Cher and Davidson[9] (1955)	$r = k[Fe^{2+}][H_2PO_4^-]^2[p_{O2}]$	4.5 $atm^{-1}mol^{-2}l^2$ hr^{-1}	Flow method flow rate: 0.5 L/min T: 303 K Titration method for iron $[Fe^{2+}]$: 3-4 X10^{-4} M	83.6
Tamuira et al.[10] (1976)	$r = k[Fe^{2+}][O_2][OH^-]^2$	2.3 X 10^{14} $M^{-3}l^{-3}sec^{-1}$	Neutral solution T: 298 K	
George[11] (1954)	$r=[Fe^{2+}]^2[O_2]$		T: 298-313 K In $HClO_4$ solution calorimetric method for iron batch	
Just[12] (1908)	$r = k[Fe^{2+}][O_2][OH^-]^2$	5.7 X 10^{13} M^{-3} sec^{-1}	Neutral solution T: 293 K	

Table IV.3.2

The literature data for Fe^{2+} oxidation with H_2O_2 in aqueous solution.

Authors	**Kinetic Equation r = 1/2 (d[Fe^{3+}]/dt)**	**Rate Constant, k (20°C)**	**Condition**	**Activation Energy, kJ/M**
Skinner, et al.[23] (1980)	$r = k[H_2O_2][Fe^{2+}]$	200 M^{-1} sec^{-1} L	Rotating T = 298K	
Baxendale, et al.[26] (1951)	$r = k[H_2O_2][Fe^{2+}]$	53 M^{-1} sec^{-1} L	T: 285-298 1N H_2SO_4 quenching with bipyridine	42.2
Po, Sutin[22] (1968)	$r = k[H_2O_2][Fe^{2+}]$	58-64 M^{-1} sec^{-1} L	1.0 N $HClO_4$; 298K	
Wells, Salam[21] (1968)	$r = k[H_2O_2][Fe^{2+}]$	50-69 M^{-1} sec^{-1} L		
Baxendale, et al.[26] (1946)	$r = k[H_2O_2][Fe^{2+}]$	52 M^{-1} sec^{-1} L	0.0025N H_2SO_4, quenching with 2,2'-bipyridyl in acetate buffer	39
Rigg, et al.[27](1954)	$r = k[H_2O_2][Fe^{2+}]$	51.4 M^{-1} sec^{-1} L	followed production of Fe^{3+} optically	35
Dainton and Sutton[28](1953)	$r = k[H_2O_2][Fe^{2+}]$	42-65 M^{-1} sec^{-1} L	quenching with ceric ion or o-phenanthroline in 0.8 N H_2SO_4	35
Haber and Weiss[17](1934)	$r = k[H_2O_2][Fe^{2+}]$	23 M^{-1} sec^{-1} L	queching with $KMnO_4$	35

Table IV.3.3

Oxidation Rate Based on Titration Data for Oxidation with H_2O_2 at 0°C

Time Interval (min.)	H_2O_2 Flow mL/min.	Amount of Fe^{2+} (mmole)	Fe^{2+} % Remaining	Amount of Fe^{2+} Oxidized (mmole)	Rate of Oxidation (mmole/min.)
0	0.34	600	100	0.00	
0-15	0.34	588.85	83.40	97.75	6.51
15-30	0.34	578.35	66.70	95.42	6.36
30-45	0.34	568.99	50.00	91.33	6.09
45-60	0.34	558.89	33.00	89.96	6.00
60-75	0.34	550.75	16.0	89.17	5.94
75-90	0.34	542.75	0.00	86.84	5.79
0	0.65	600	100	0.00	
0-7	0.65	570.87	84.50	94.19	13.45
7-14	0.65	560.06	67.80	86.15	12.31
14-21	0.65	550.14	51.20	88.13	12.59
21-28	0.65	542.69	33.60	91.88	13.12
28-35	0.65	535.40	16.40	87.24	12.46
35-42	0.65	529.81	0.00	82.22	11.75
0	1.15	600	100	0.00	
0-3	1.15	593.10	83.54	97.62	32.54
3-6	1.15	585.20	67.51	92.51	30.84
6-9	1.15	578.09	48.33	108.57	36.19
9-12	1.15	572.09	30.56	98.56	32.85
12-15	1.15	564.89	12.50	97.02	32.34
15-18	1.15	558.09	0.00	63.81	
0	3.37	600	100	0.00	
0-3	3.37	593.52	63.29	217.88	72.63
3-6	3.37	585.62	29.44	195.33	65.11
6-9	3.37	577.47	0.00	164.26	

Table IV.3.4

Oxidation Rates Based on Titration Data for Conversion with Oxygen at 0°C

Time Interval (min.)	O_2 Flow mL/min.	Amount of Fe^{2+} (mmole)	Fe^{2+} % Remaining	Amount of Fe^{2+} Oxidized (mmole)	Rate of Oxidation (mmole/min.)
0	75	600	100	0.00	
0-7	75	593.32	92.00	47.47	6.78
7-14	75	582.96	83.00	51.63	7.38
14-21	75	573.29	70.00	72.88	10.41
21-28	75	564.38	52.50	96.10	13.80
28-35	75	555.55	34.00	96.58	13.80
35-42	75	546.17	20.00	72.28	10.32
42-49	75	536.94	9.00	51.68	7.38
49-56	75	527.55	0.00	38.93	5.56
0	185	600	100	0.0	
0-3	185	593.69	94.30	32.1	10.7
3-8	185	584.48	82.36	71.0	14.2
8-13	185	575.88	65.10	98.0	19.6
13-18	185	566.93	46.01	105.0	21.0
18-23	185	557.41	26.78	102.0	20.4
23-28	185	549.06	10.46	99.0	19.8
28-33	185	541.66	0.00	56.5	11.3
0	390	600	100		
0-3	390	592.55	90.00	59.26	19.75
3-8	390	582.95	71.00	109.79	21.96
8-13	390	573.45	43.50	132.95	26.59
13-18	390	564.35	18.50	135.94	27.19
18-23	390	555.35	6.10	61.53	12.31
23-28	390	545.55	0.00	13.17	

Table IV.3.5

Surface Area and Porosity of Samples Prepared by Oxidation with H_2O_2 or O_2 (1M Fe^{2+}, 0°C, $Fe^{2+}/OH^- = 0.4$)

Oxidant	Flow Rate mL/min.	BET Surface Area, m^2/g	Pore Volume mL/g	$(dV/dR)_{max}$, nm
H_2O_2	0.34	84	0.462	12.7
H_2O_2	0.66	167	0.532	7.2
H_2O_2	1.67	148	0.436	6.8
H_2O_2	3.37	156	0.524	9.1
O_2	74	191	0.463	5.2
O_2	185	185	0.428	4.9
O_2	390	201	0.688	7.6
O_2	780	83	0.606	13.4

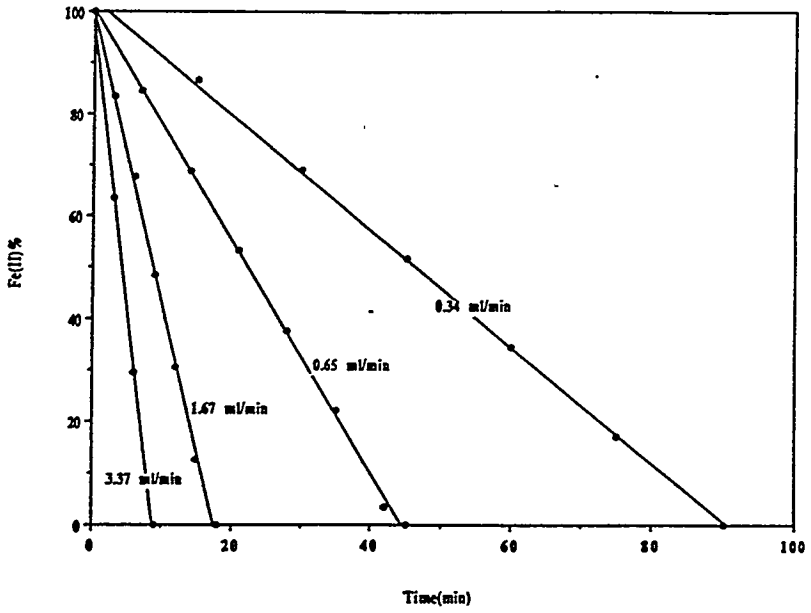

Figure IV.3.1. The change in the amount of Fe^{2+} remaining versus time of flow of hydrogen peroxide (initial $Fe^{2+}/OH^- = 0.4$, 1M Fe^{2+}, 10.2 M H_2O_2, 273K, 1 atm.).

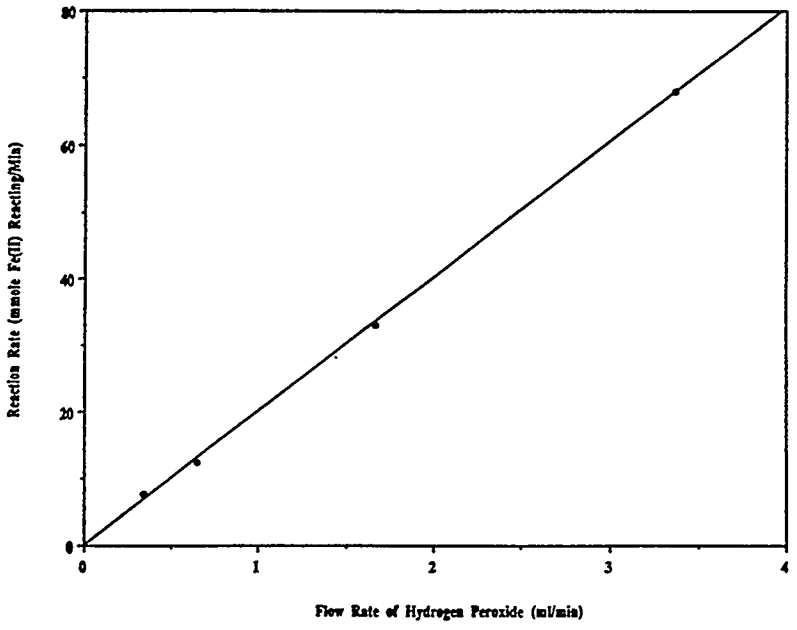

Figure IV.3.2. The dependence of the reaction rate for Fe^{2+} oxidation upon hydrogen peroxide flow rate.

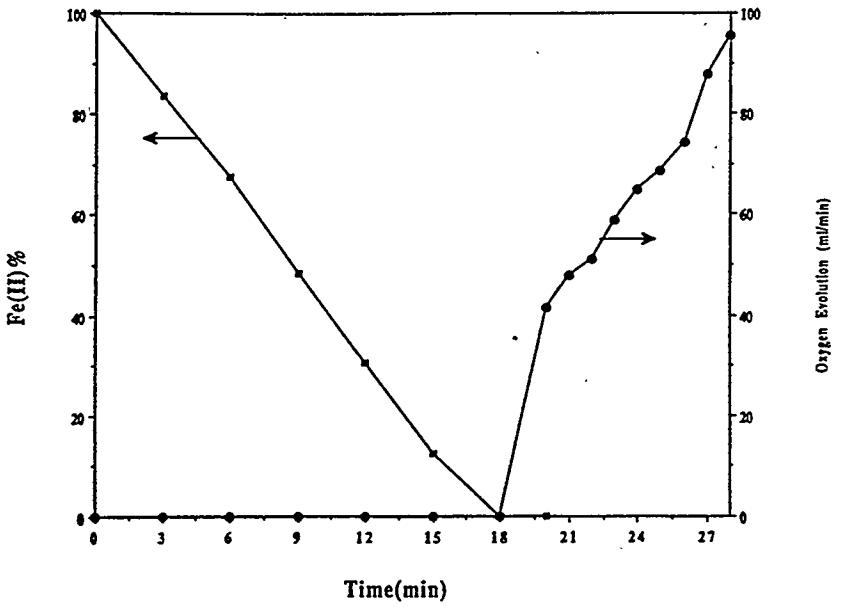

Figure IV.3.3. A comparison of the oxidation of Fe^{2+} and the evolution of gaseous oxygen with increasing time of addition of hydrogen peroxide.

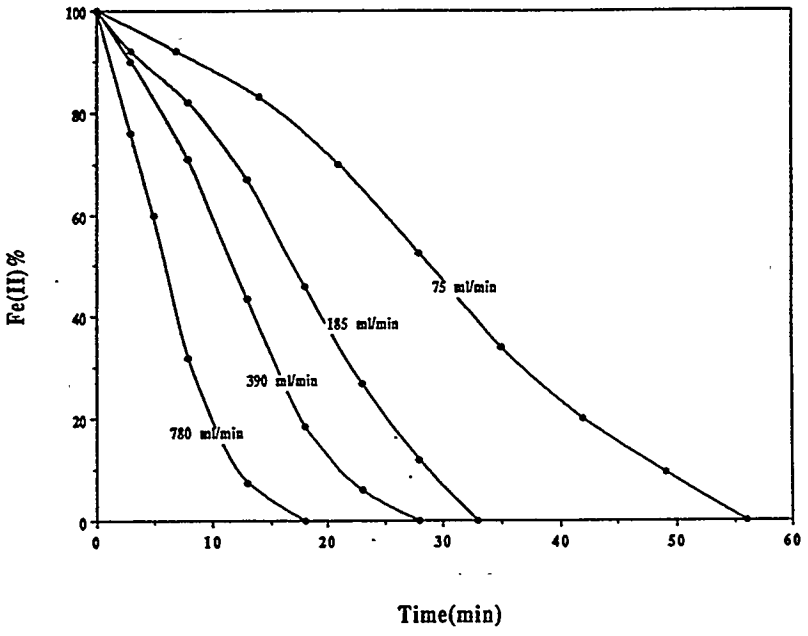

Figure IV.3.4. The change in the amount of Fe^{2+} remaining versus time of flow of oxygen (initial Fe^{2+}/OH^{-} = 0.4, 1M Fe^{2+}, 10.2 M H_2O_2, 273K, 1 atm.).

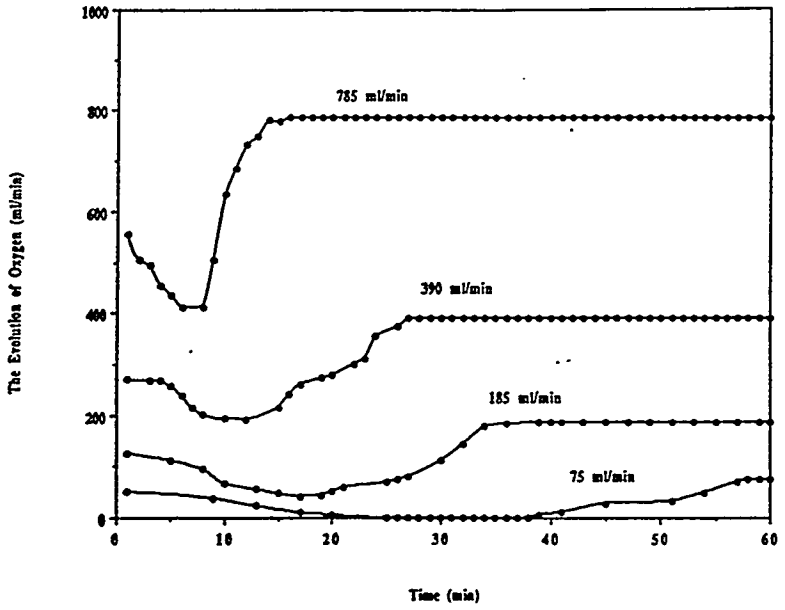

Figure IV.3.5. Flow of gas exiting the reactor for various inlet flows of oxygen.

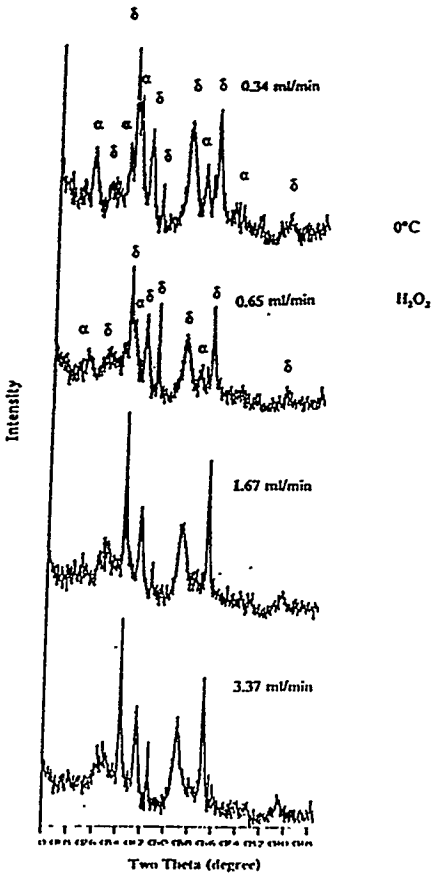

Figure IV.3.6. The effect of the rate of H_2O_2 addition upon the XRD patterns (α- and δ-FeOOH major peaks indicated, rate of H_2O_2 addition indicated for each XRD pattern).

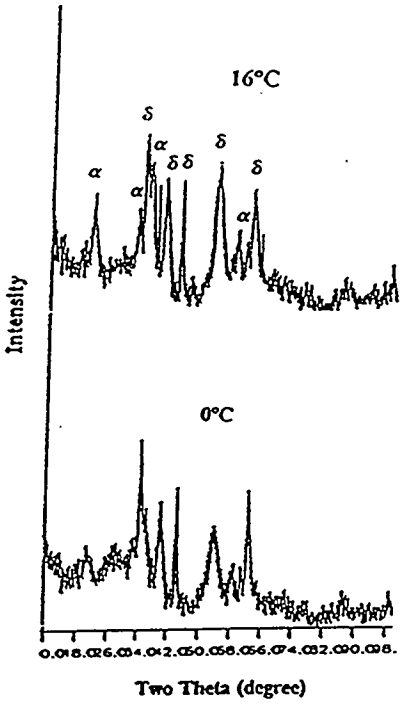

Figure IV.3.7. The effect of the rate of oxygen addition upon the XRD patterns (α- and δ-FeOOH major peaks indicated, rate of oxygen flow indicated for each XRD pattern.

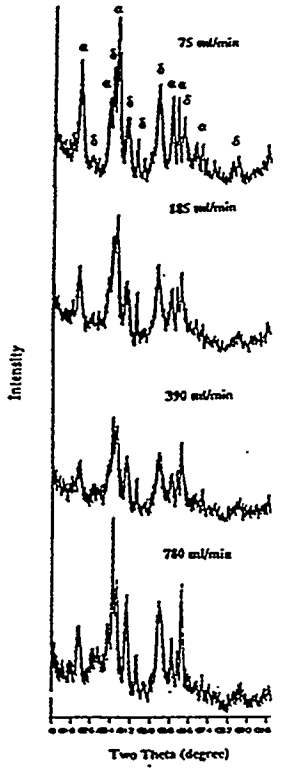

Figure IV.3.8. XRD diffraction patterns prepared under identical conditions (initial $Fe^{2+}/OH^- = 0.4$, 1M Fe^{2+}, 1 atm. 0.65 mL H_2O_2/min.) except temperature (289K upper curve, 273K bottom curve).

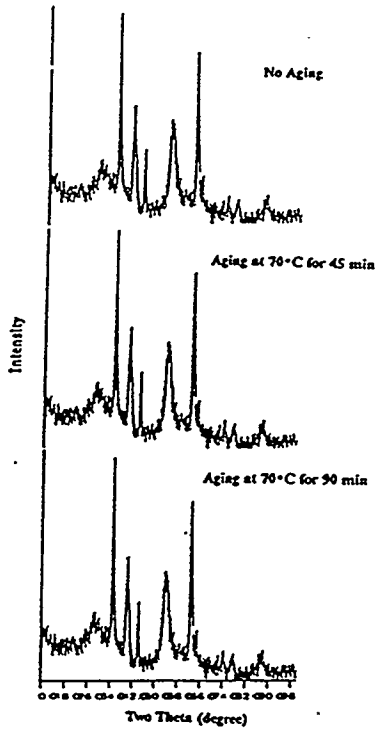

Figure IV.3.9. XRD patterns of a material collected following precipitation at 298K (no aging, top curve) and after aging at 343K for 45 min. (middle curve) and 90 min. (bottom curve) (initial Fe^{2+}/OH^{-} = 0.4, 1M Fe^{2+}, 1 atm.).

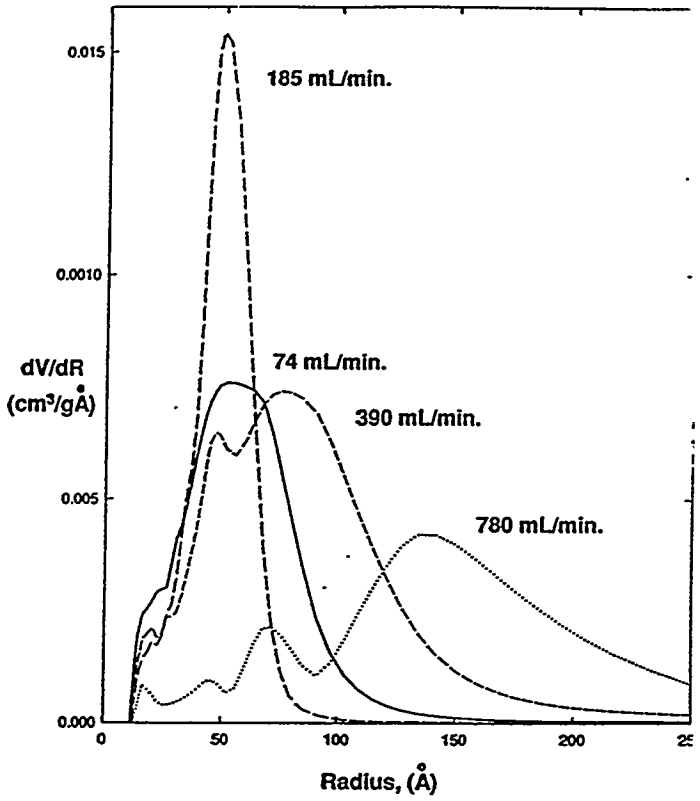

Figure IV.3.10. Pore size distribution of samples (dried at 343K) prepared by oxidizing Fe^{2+} at 273K using different flow rates of H_2O_2 (initial Fe^{2+}/OH^{-} = 0.4, 1M Fe^{2+}, 10.2 M H_2O_2, 273K, 1 atm.).

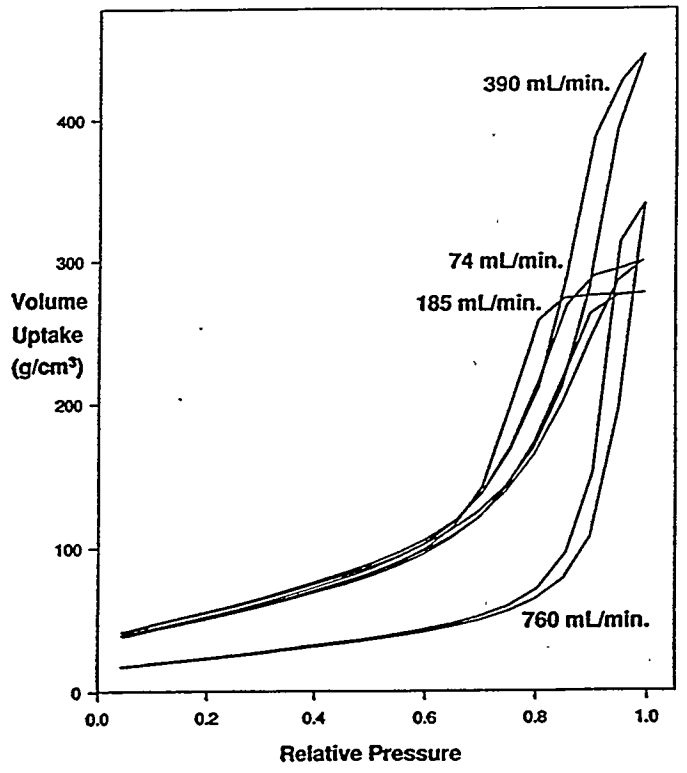

Figure IV.3.11. Nitrogen adsorption/desorption isotherm of samples (dried at 343K) prepared by oxidizing Fe^{2+} at 273K using different flow rates of H_2O_2 (initial $Fe^{2+}/OH^- = 0.4$, 1M Fe^{2+}, 10.2 M H_2O_2, 273K, 1 atm.).

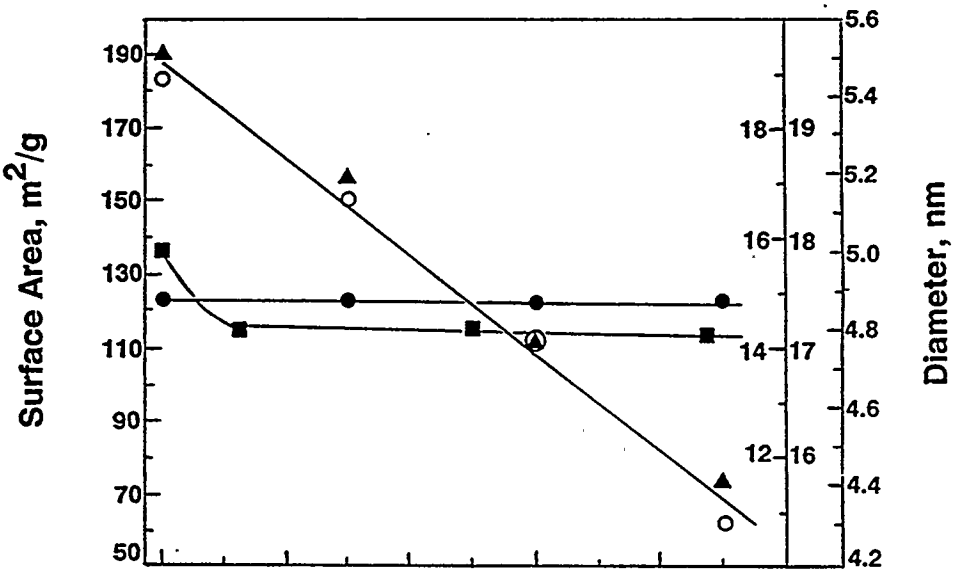

Figure IV.3.12. Comparison of surface area (■) and crystal dimension in direction of 112 (●) and 100 (▲) (12-18 nm axis) and 102 (○) (4.4-5.6 axis) planes of an unaged sample and samples aged for increasing times at 343K.

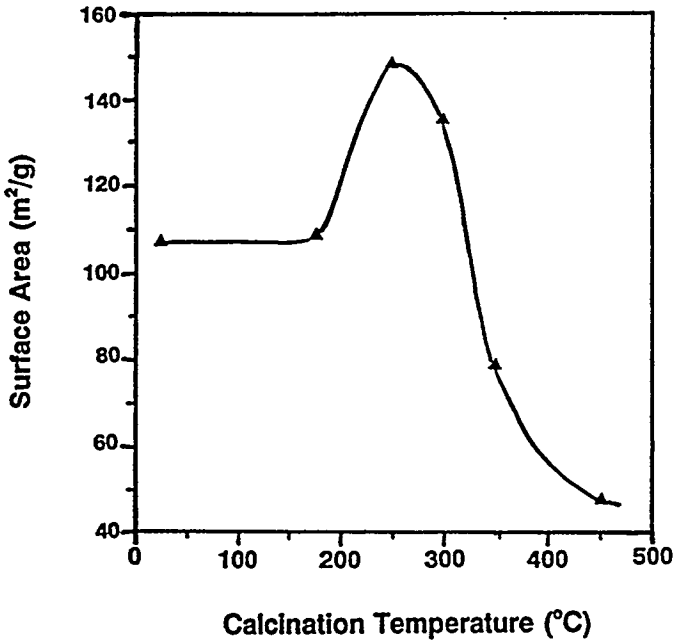

Figure IV.3.13. The effect of calcination temperature on the surface area of δ-FeOOH.

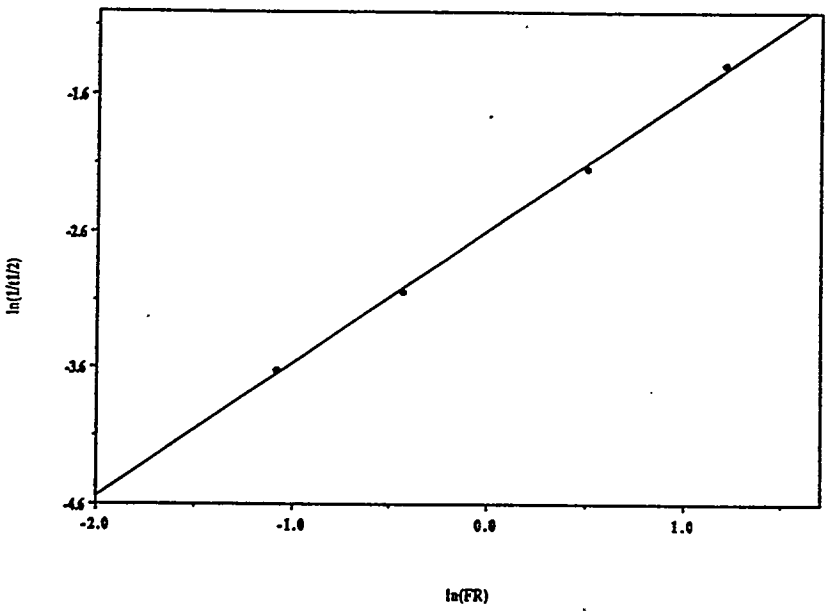

Figure IV.3.14. Plot of the ln (time for 50% Fe^{2+} oxidation) versus ln(flow rate) of hydrogen peroxide.

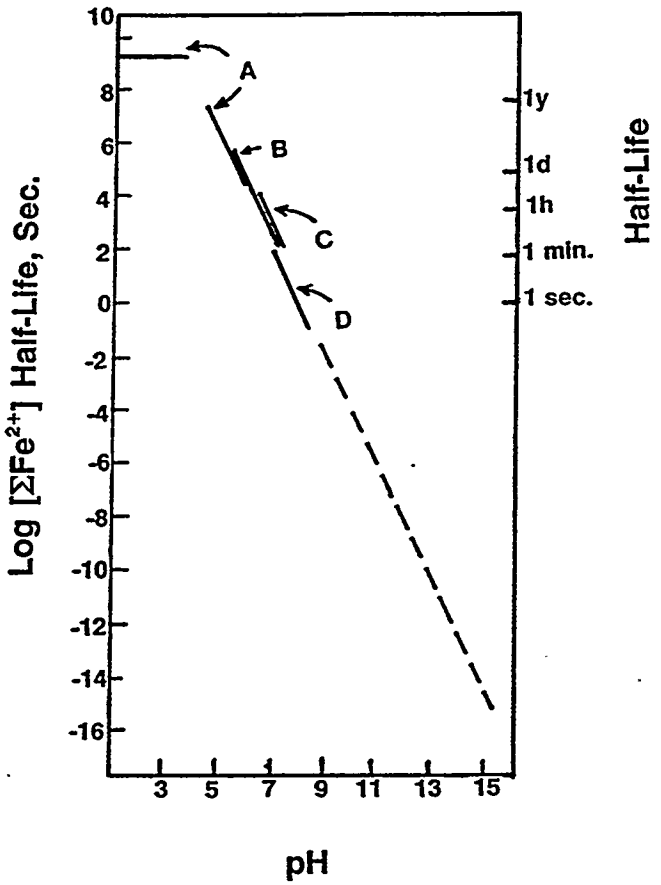

Figure IV.3.15. Plot of literature data (36-40; A, 36; B, 37; C, 38; D, 39) data for the half-life for Fe^{2+} oxidation as a function of the pH of the solution or slurry.